PYGMY DIPOLE RESONANCE IN Sn ISOTOPES AND ITS ASTROPHYSICAL IMPACT*

Maria Markova, Ann-Cecilie Larsen
Frank Leonel Bello Garrote

Department of Physics, University of Oslo, 0316 Oslo, Norway

Received 12 December 2024, accepted 18 December 2024, published online 10 April 2025

The low-lying electric dipole strength in $^{111-113,116-122,124}$Sn was extracted with the Oslo method to systematically investigate the pygmy dipole resonance (PDR) and its evolution in Sn isotopes. The nuclear level densities (NLD) and the γ-ray strength functions (GSF) obtained from the Oslo data were used as inputs in the TALYS reaction code to produce radiative neutron-capture cross sections, Maxwellian-averaged cross sections, and rates relevant for the heavy-element nucleosynthesis. Despite a relatively small observed impact of the PDR, the experimentally extracted ^{121,123}Sn(n,γ) ^{122,124}Sn cross sections provide a notable reduction of a currently available theoretical uncertainty for the abundances of Sb isotopes in the i-process simulations.

DOI:10.5506/APhysPolBSupp.18.2-A3

1. Introduction

The pygmy dipole resonance (PDR) is commonly observed as an enhancement of the low-lying electric dipole strength on top of the isovector giant dipole resonance (IVGDR) in the vicinity of the neutron separation energy in stable and unstable heavy nuclei. Even though the degree of its collectivity still remains a matter of debates, the vast majority of studies revolve around the PDR nature being linked to the oscillations of the neutron excess *versus* the isospin-saturated core [1]. This connection further implies that any experimental constraints on the PDR strength might potentially provide useful insights into the neutron skin properties in heavy nuclei and the nuclear equation of state [2]. Furthermore, this low-energy enhancement was suggested to boost the radiative neutron-capture cross sections, which might further affect the production of elements in the heavy-element nucleosynthesis [3].

* Presented at the 57$^{\text{th}}$ Zakopane Conference on Nuclear Physics, *Extremes of the Nuclear Landscape*, Zakopane, Poland, 25 August–1 September, 2024.

Even with a plethora of currently available techniques and complementary probes, a clear consistent experimental picture of the evolution of the PDR and the low-lying $E1$ strength in general is still absent. In addition to the nuclear structure aspects, such experimental information is crucial for constraining the model inputs used in large-scale simulations of astrophysical s, r, and i processes. In this work, we present a systematic study of the low-lying electric dipole strength in eleven Sn isotopes using the Oslo method. The latter allows us to access both the nuclear level densities (NLD) and γ-ray strength functions (GSF), two crucial ingredients in (n, γ) cross-section calculations within the statistical model, and thus, address the potential astrophysical role of the low-lying E1 strength connected to the PDR. In particular, a recent study exploring the impact of uncertainties associated with theoretical reaction rates on the i-process elemental production revealed that the (n, γ) rates and their uncertainties for several Sn isotopes close to the stability might have a relatively high local impact on the i-process flow [4]. Since these isotopes of potential interest are part of the present systematic study, this matter will be also covered in the following sections.

2. Experiments and the Oslo method

The Oslo method is a widely used technique for a simultaneous extraction of such statistical properties of excited nuclei as NLDs and GSFs below the neutron separation energy, where the PDR is expected to be observed. Both of these characteristics are extracted from particle–γ coincidence data obtained in light-particle-induced reactions. In this work, eleven tin isotopes ($^{111-113,116-122,124}$Sn) were studied with p, d, and ^{3}He beams in several experimental campaigns at the Oslo Cyclotron Laboratory (OCL) from 2003 to 2022. In the earlier experiments, the CACTUS γ ball consisting of 28 $5'' \times 5''$ NaI(Tl) detectors was used. The most recent experiments on ^{117,119,120,124}Sn were performed with a scintillator array OSCAR, consisting of 30 large-volume $LaBr_3$(Ce) detectors. Switching to the new detecting system allowed us to exploit much higher efficiency of the setup, improved energy resolution, and excellent timing properties of $LaBr_3$(Ce) detectors, crucial for coincidence measurements. Particle events were recorded with a custom-designed Si telescope ring (SiRi), made of eight 1500 μm thick E and 64 segments of $\approx$140 μm thick ΔE counters. The earliest experiments were performed with SiRi placed in the forward position, covering angles from 40° to 54°, while in the most recent experiments, it covered from 126° to 140° in the backward position. The energy deposited in the E and ΔE particle detectors was converted into the initial excitation energy E_i of the residual nucleus with the typical excitation energy resolution being $\approx$ 100–300 keV.

The ^{112,117,119,120,122,124}Sn targets were studied in the (p,p'), (p,d), (d,p), (^{3}He, ^{3}He$'$), and (^{3}He, α) reactions with 16 and 25 MeV protons, 11.5 MeV deuterons, and a 38 MeV ^{3}He beam. More information on the experimental conditions is provided in Ref. [5].

Particle–γ coincidence data were extracted for the excitation energies up to the neutron threshold (S_n) in the studied nuclei. At each excitation energy, γ-ray spectra were unfolded using the CACTUS and OSCAR detector responses. As a next step, all second- and higher-order transitions in the observed γ cascades were removed by applying the iterative first-generation method, outlined in detail in Ref. [6]. The first-generation data for Sn isotopes selected for the further analysis correspond to $E_\gamma \gtrsim$ 1–2 MeV and initial excitation energies from 3–5 MeV to S_n due to the limitations of this procedure and the underlying assumptions of the Oslo method [6].

The principal idea of the Oslo method is based on the proportionality of the first-generation γ-ray distribution to the γ transmission coefficient $\mathcal{T}_{\mathrm{i}\to\mathrm{f}}$ and the density of final levels ρ_f, supported by both Fermi's golden rule and the Hauser–Feshbach theory (see [5] and references therein). This corresponds to the following decomposition of the first generation matrix $P(E_\gamma, E_\mathrm{i})$ within the above-mentioned E_γ and E_i limits

$$P(E_\gamma, E_\mathrm{i}) \propto \mathcal{T}_{\mathrm{i}\to\mathrm{f}}\, \rho_\mathrm{f}\,. \tag{1}$$

This relation is expected and was shown (see *e.g.* [6]) to hold well for the compound excited states within the chosen excitation energies. The Brink–Axel hypothesis is assumed to disentangle the functional forms of the NLD and GSF, proportional to the γ-transmission coefficient [7]. Finally, to extract the physical solutions, these functional forms are normalized using experimental neutron-resonance data and their systematics. In particular, the slope of the NLD and GSF is determined from the experimental value of the average neutron-resonance spacing. Additionally, the absolute values of the NLD are adjusted to available low-lying tabulated discrete states, and the absolute values of the GSF are constrained with the average total radiative width from neutron resonance studies. A more detailed description of this procedure, the discussion of the normalization parameters, and their values for the Sn isotopes are provided in [5].

3. Results and discussions

3.1. Nuclear level density, γ-ray strength function, and the PDR in Sn isotopes

Following the procedure from the previous section, the NLDs and GSFs were extracted for all of the studied Sn isotopes. Figure 1 presents both of

these characteristics extracted with the Oslo method from the ^{120}Sn$(p, p'\gamma)$ experiment for the ^{120}Sn isotope. The $\rho(S_n)$ value from the neutron-resonance data used for the normalization is also shown in Fig. 1 (a). The results for other isotopes are provided in Ref. [5]. The NLDs of other even–even isotopes are in good agreement with that of ^{120}Sn; all of them reproduce the low-lying discrete states well up to ≈ 3 MeV and follow a clear constant-temperature trend. The GSFs of all the isotopes are quite similar in shape, and the typical example is shown in Fig. 1 (b) for ^{120}Sn. All of the strengths are in good agreement with available (γ, n) data and, in particular, the (p, p') data from the recent Coulomb excitation study of even–even Sn isotopes in forward angle relativistic proton scattering [8] (see Fig. 1 (b)). All of the strengths point at the presence of a resonance-like enhancement in the vicinity of the neutron separation energy, at ≈ 8.0–8.5 MeV, commonly interpreted as the PDR.

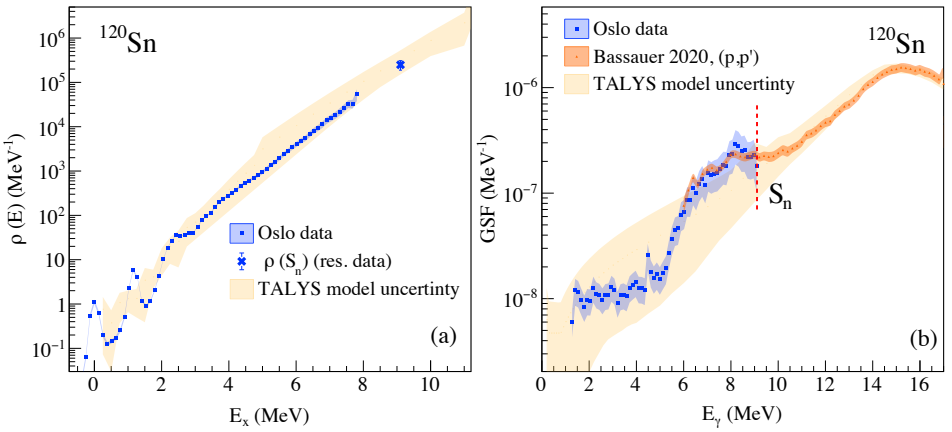

Fig. 1. (a) The NLD of ^{120}Sn extracted with the Oslo method shown together with the TALYS model uncertainty band. (b) The same as (a) but for the GSF. A vertical dashed line marks the neutron threshold energy in ^{120}Sn.

The Oslo method GSF is extracted assuming the dominant dipole character of γ transitions from the quasi-continuum excitation energy region. Moreover, the method does not distinguish between electric and magnetic types of transitions. Combining the Oslo data with the electric and magnetic GSFs from the relativistic Coulomb excitation experiment [8] allows for a decomposition of the total dipole strength in terms of the giant dipole resonance, the low-lying E1 strength and the spin-flip M1 component as outlined in detail in Ref. [5]. Based on a parameterization by a single or double Gaussian function as shown in Ref. [5], the low-lying E1 strength exhausts $\approx$ 2–3% of the classical Thomas–Reiche–Kuhn (TRK) sum rule.

This value is observed throughout the whole chain of stable Sn isotopes and does not change in any significant way with the increasing neutron excess, as expected within the neutron skin oscillation picture of the PDR [1]. The total electric dipole strength confined within 4–10 MeV exhausts ≈ 3.2–4.2% of the TRK sum rule, and the contribution from the IVGDR to this value is ≈ 1.5% TRK. None of the GSF models available in the TALYS reaction code [9] are able to reproduce this enhancement and an overall shape of the experimental GSFs. Moreover, they tend to disagree with each other below the neutron separation energy in absolute values and shapes, forming a broad uncertainty band, shown in Fig. 1 (b) for ^{120}Sn.

3.2. Radiative neutron-capture cross sections in i-process simulations

The newly extracted NLDs and GSFs of Sn isotopes were further used as inputs in combination with the phenomenological optical model potential of Koning and Delaroche [9] in the TALYS reaction code to produce (n, γ) cross sections and Maxwellian-averaged cross sections (MACS) (see Ref. [5] for more details). An example of the obtained results for ^{120}Sn is shown in Fig. 2. Large spans of model uncertainties for the NLD and GSF, currently available in TALYS, are inevitably propagated in large uncertainty bands of the cross sections, also shown in Fig. 2. The cross sections extracted with the Oslo inputs agree nicely with other available experimental

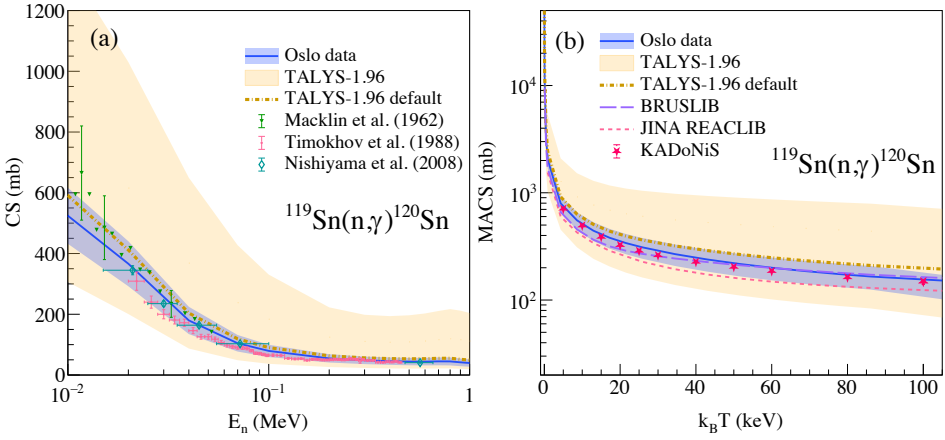

Fig. 2. (a) Radiative neutron-capture cross sections extracted with the Oslo method data for ^{120}Sn. The cross sections are shown together with the TALYS model uncertainty band and other experimental results by Macklin *et al.* [10], Timokhov *et al.* [11], and Nishiyama *et al.* [12]. (b) Maxwellian-averaged cross section for the same reaction, shown with the TALYS model uncertainty band, the cross sections from JINA REACLIB [13], BRUSLIB [14], and KADoNiS [15] libraries.

data, as shown in Fig. 2 (a), which serves as an additional indirect check of the Oslo method normalization procedure. Furthermore, the MACS agree fairly well with the cross sections and rates available in JINA REACLIB [13], BRUSLIB [14], and KADoNiS [15] libraries for most of the cases (provided in [5]). The 8 MeV enhancement ($\approx$ 2–3% of the TRK sum rule) of the electric dipole strength clearly observed in the Oslo GSFs corresponds to an approximately 20% contribution to the total MACS in the heaviest studied Sn isotopes at $k_{\mathrm{B}}T \approx 30$ keV. Even though this impact is quite small, especially when considering the experimental uncertainty bands, the newly extracted GSFs in combination with the corresponding NLDs allow for a significant reduction of the model uncertainties for the (n,γ) cross sections, as shown in Fig. 2. In addition to the uncertainty associated with different TALYS model combinations, the uncorrelated parameter uncertainties have also been suggested in Ref. [4] to have a certain impact on, in particular, i-process simulations. In this case, they were estimated using the Hartree–Fock–Bogolubov (HFB)+combinatorial NLD and D1M+quasi-particle random phase approximation (QRPA) GSF models according to the procedure outlined in Ref. [4]. The obtained parameter uncertainty bands are shown in Fig. 3 together with the model and experimental uncertainties for the (n,γ) reaction rates for the heaviest studied ^{122,124}Sn isotopes.

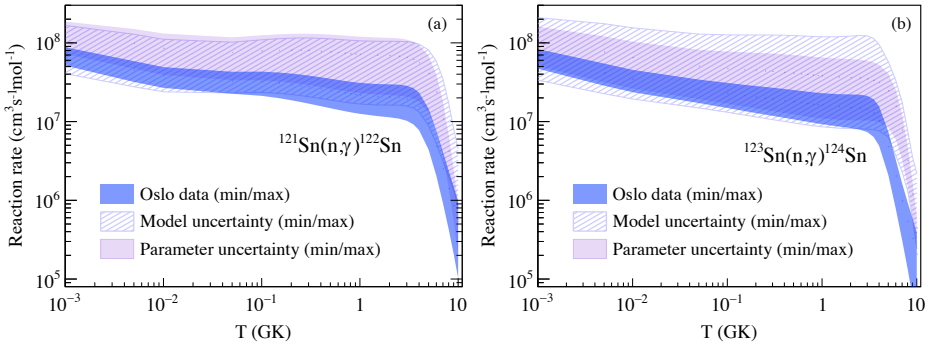

Fig. 3. (Color online) Uncertainty bands for the neutron-capture rates in the (a) ^{121}Sn(n,γ) ^{122}Sn and (b)^{123}Sn(n,γ) ^{124}Sn reactions. The dark blue/gray band corresponds to the span of experimentally constrained reaction rates. The hatched band denotes the span of the TALYS model uncertainty. The pale purple/light gray band is due to the variation of the model parameters according to [4] (parameter uncertainty).

The impact of all of the above-mentioned uncertainties in the cases of the ^{121,123}Sn$(n,\gamma)^{122,124}$Sn reactions was estimated in the performed simulations of the i-process nucleosynthesis in a 1 $M_{\odot}$ low-metallicity ([Fe/H] $= -2.5$)

asymptotic giant branch model computed with the STAREVOL code [5]. Figure 4 shows the resulting abundances of produced isotopes in the Sn mass region. The uncertainties associated with the theoretical model and parameter uncertainties and experimental uncertainties of the ^{121,123}Sn$(n,\gamma)^{122,124}$Sn reaction rates are shown as hatched and solid bands in Fig. 4 (a) and as a solid band Fig. 4 (b), respectively. The impact of the newly constrained rates is local, affecting mainly the production of the ^{121,123}Sb isotopes. With the new experimental inputs on ^{122,124}Sn, the overall uncertainty for the production of the ^{121}Sb (^{123}Sb) isotope is reduced from 0.75 (0.98) to 0.29 (0.26) dex.

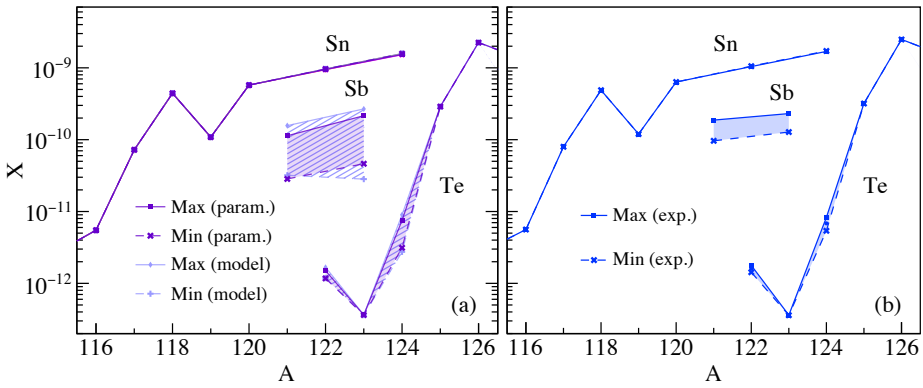

Fig. 4. (Color online) Isotopic mass fraction X as a function of the mass number A, around the Sn region of multizone AGB stellar models experiencing i-process nucleosynthesis, computed with different combinations of ^{121,123}Sn(n,γ) rates. (a) Model (hatched area) and parameter (pale purple/light gray area) uncertainty bands calculated using the corresponding uncertainty limits from Fig. 3. (b) The same for the experimental uncertainties.

4. Conclusion

The low-lying electric dipole strength was studied in terms of the γ-ray strength function for eleven Sn isotopes with the primary goal of investigating its evolution with increasing neutron number. The low-energy enhancement observed at $\approx$ 8 MeV in all of the isotopes exhausts $\approx$ 2–3% of the TRK sum rule and does not increase with increasing proton–neutron asymmetry, in contradiction with the majority of theoretical predictions. To address the importance of statistical nuclear inputs below the neutron threshold for astrophysical calculations, the NLDs and GSFs of the studied isotopes were used to extract the radiative neutron-capture cross sections

using the TALYS reaction code. Even though the observed enhancement has a contribution to the total cross sections compatible with the experimental uncertainties, the new experimental GSFs and NLDs might potentially help to single out some of the models in astrophysical calculations, which reproduce the experimental data well and can be relied on away from the stability. Moreover, the newly constrained cross sections allowed us to notably reduce the parameter and model uncertainties of abundances for several Sb isotopes in the i-process simulations.

REFERENCES

[1] E. Lanza, L. Pellegri, A. Vitturi, M.V. Andrés, *Prog. Part. Nucl. Phys.* **129**, 104006 (2023).

[2] LAND Collaboration (A. Klimkiewicz *et al.*), *Phys. Rev. C* **76**, 051603(R) (2007).

[3] S. Goriely, *Phys. Lett. B* **436**, 10 (1998).

[4] S. Martinet, A. Choplin, S. Goriely, L. Siess, *Astron. Astrophys.* **684**, A8 (2024).

[5] M. Markova *et al.*, *Phys. Rev. C* **109**, 054311 (2024).

[6] A.C. Larsen *et al.*, *Phys. Rev. C* **83**, 034315 (2011).

[7] M. Markova *et al.*, *Phys. Rev. Lett.* **127**, 182501 (2021).

[8] S. Bassauer *et al.*, *Phys. Rev. C* **102**, 034327 (2020).

[9] A. Koning, S. Hilaire, S. Goriely, *Eur. Phys. J. A* **59**, 131 (2023).

[10] R.L. Macklin, T. Inada, J.H. Gibbons, *Nature* **194**, 1272 (1962).

[11] V.M. Timokhov *et al.*, *Sov. J. Nucl. Phys.* **50**, 375 (1989).

[12] J. Nishiyama *et al.*, *J. Nucl. Sci. Technol.* **45**, 352 (2008).

[13] R.H. Cyburt *et al.*, *Astrophys. J. Suppl.* **189**, 240 (2010).

[14] Y. Xu *et al.*, *Astron. Astrophys.* **549**, A106 (2013).

[15] I. Dillmann *et al.*, data extracted using the KADoNiS on-line data service, `https://exp-astro.de/kadonis1.0/index.php`. Last accessed: November 1, 2024.